A spectroscopic-imaging scanning tunneling microscope in vector magnetic field

Lihui Zhou*,[1] Qingyu He,[1] Xinglu Que,[1] Andreas W. Rost,[1,2] and Hide Takagi[1,*]

[1] *Max Planck Institute for Solid State Research, Heisenbergstrasse 1, Stuttgart, 70569, Germany*

[2] *SUPA, School of Physics and Astronomy, University of St Andrews, North Haugh, St Andrews, Fife, KY16 9SS, UK*

Abstract

Cryogenic scanning tunneling microscopy and spectroscopy (STM/STS) performed in a high vector magnetic field provide unique possibilities for imaging surface magnetic structures and anisotropic superconductivity and exploring spin physics in quantum materials with atomic precision. Here we describe the design, construction, and performance of a low-temperature, ultra-high-vacuum (UHV) spectroscopic-imaging STM equipped with a vector magnet capable of applying a field of up to 3 T in *any* direction with respect to the sample surface. The STM head is housed in a fully bakable UHV compatible cryogenic insert and is operational with a variable temperature ranging from ~ 300 K down to 1.5 K. The insert can be easily upgraded using our home designed ^{3}He refrigerator. In addition to layered compounds which can be cleaved at a temperature of either ~ 300 K, ~ 77 K, or ~ 4.2 K to expose an atomically flat surface, thin films can also be studied by transferring using a UHV suitcase directly from our oxide thin-film lab. Samples can be further treated with a heater and a liquid helium/nitrogen cooling stage on a three-axis manipulator. STM tips can be treated *in vacuo* by e-beam bombardment as well as ion sputtering. We demonstrate the successful operation of the STM with varying the magnetic field direction. Our facility provides a way to study materials where the magnetic anisotropy is a key factor in determining the electronic properties such as topological semimetals and superconductors.

* The authors to whom correspondence may be addressed: lihui.zhou.cn@gmail.com, h.takagi@fkf.mpg.de.

I. INTRODUCTION

Scanning tunneling microscopy (STM), invented by Binnig and Rohrer [1, 2], enables to image sample surfaces at the atomic scale and to directly probe local electronic density of states (LDOS) by scanning tunneling spectroscopy (STS). It has been playing an ever increasingly important role in the investigation of the correlation between structural and electronic properties of materials, with unprecedentedly high resolution in real space. Ever since its invention, STM operating at a low temperature in a magnetic field has been widely utilized to study novel electronic properties and explore emergent quantum phases in materials of e.g. superconductors, magnetic thin films, and topological materials [3–9]. Many interesting phenomena have been revealed such as spin coupling between individual adatoms [10, 11], interplay of magnetism and superconductivity at the single-atom level [9, 12, 13], and density wave states in cuprates [14]. More recently, materials with strong spin-orbit coupling (SOC) such as topological insulators, topological semimetals, and magnetic thin films hosting skyrmion, have attracted intensive attentions [15–22]. They have inherent novel electronic properties that strongly depend on the underlying spin textures, thus promising for nanoscale spintronics applications. For such spin-orbit-entangled materials, cryogenic STM operating in a magnetic field in any spatial direction is highly desired to manipulate and map the three-dimensional spin structures, thus as well as the electronic structures.

While a few home-built STMs equipped with commercially available vector magnets have been successfully built [23–29], fully UHV compatible STM setups, working at a temperature below the liquid helium boiling point and in a field in excess of 2 T in *arbitrary* direction, are still rare [30]. In this paper we present a home-built UHV STM operating in a magnetic field with variable direction with a base temperature of ~ 1.5 K. We use a 2D horizontally rotatable instead of bulky 3D vector magnet assembly, enabling a larger in-plane field and longer measurement time due to the reduced helium boil-off. The capability to apply a magnetic field of up to 3 T in any direction, in addition to 9 T perpendicular to the sample surface, allows for the manipulation and atomic scale imaging of surface spin texture in all three spatial directions, thus enabling the study of the interplay of electronic and magnetic structures in quantum materials. The measurement temperature is variable ranging from

$\sim 300\,\mathrm{K}$ down to $1.5\,\mathrm{K}$ and allows for tracking the evolution of electronic phases as a function of the temperature. Upgrade with a home-built ^{3}He refrigerator is feasible. Moreover, the facility is particularly suitable to study thin films grown by our oxide thin-film lab which can be transferred with a fully UHV compatible transport technique to avoid surface contamination.

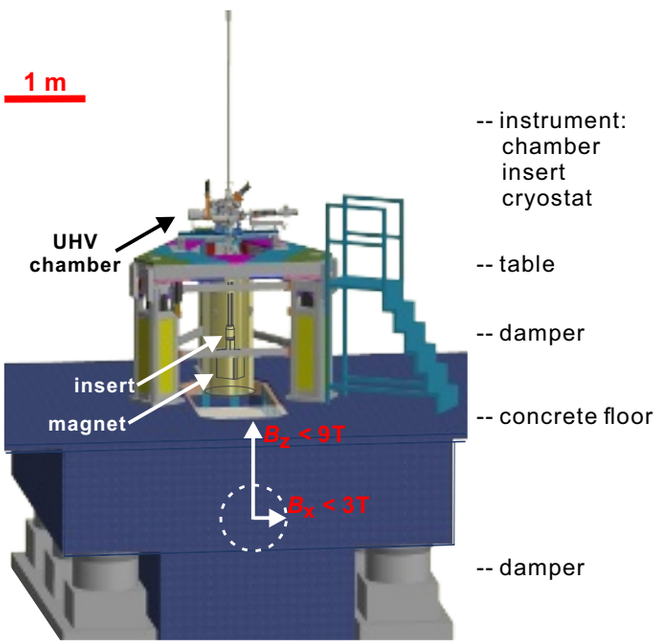

FIG. 1. Schematic of the overall structure of our facility. The laboratory is built on a concrete floor (dark blue) floating on the first set of air dampers (grey) sitting on a separate basement. The instrument consisting of UHV chambers, a cryogenic insert containing the STM unit, and a liquid helium dewar, is placed on a table supported by the second set of air dampers sitting on the concrete floor. The STM insert is housed in the dewar where the vector magnet is placed. The magnetic field relative to the facility is schematically shown. A field of up to 3 T can be applied in any direction determined by the circular orbit (dashed circle, see Fig. 4**(a)** for details).

II. ENVIRONMENT

The working principle of STM is the quantum tunneling of electrons across the potential barrier between the tip and sample which exponentially depends on the barrier width [1, 2]. To obtain high-quality topographic and spectroscopic data, the tip-sample

separation should therefore be maintained with (sub-)picometer scale stability. To this end, great care must be taken to reduce all acoustic, vibrational, and electrical noise from the immediate environment. This is a necessary prerequisite condition for the successful operation of an STM setup. Our laboratory is located in the specially designed Precision Laboratory at Max Planck Institute in Stuttgart, which provides an acoustically, seismically, and electromagnetically shielded environment. The instrumentation room is made of soundproof concrete with multiple walls, and 60 dB attenuation of acoustic noise is achieved.

Vibration attenuation is achieved with a multi-stage isolation concept (see Fig. 1). The instrumentation room is built on a separate basement, sitting on which are six pneumatic dampers (grey) supporting a glass-fiber reinforced concrete block (blue) of ~ 150 ton weight. This first set of pneumatic dampers can work flexibly either in a passive or active mode. On the concrete we built a second passive pneumatic system to suspend a ~ 1 ton heavy triangular table made of rigid aluminum. The whole instrument, consisting of UHV chambers, a cryogenic insert containing the STM head, and a liquid helium dewar housing the vector magnet, is then supported by the table. All roughing pumps including the one for the 1 K cooling system are placed in a separate room tens of meters away.

Electromagnetic noise isolation with 100 dB attenuation down to 40 GHz is achieved by shielding the room with a closed metal shell. All electrical cables entering the room are filtered at the wall. The noise is further reduced by filtering the cables, except the one carrying the tunneling current, entering the cryogenic insert at the feedthroughs on top of the cryostat. To avoid any potential grounding loop, we use a star ground configuration with the cryostat top as the anchoring point. During measurement all electronic controllers except the one for the STM are switched off, and good vacuum is maintained only through the cryo-pumping effect of the cold wall of the cryogenic insert.

We use SPECS Nanonis RC5/SC5 to control the STM unit and an ultra-low noise Femto LCA-1K-5G preamplifier to detect the tunneling current. The modulated signal is recorded by the digital lock-in amplifier implemented in the RC5/SC5 electronics. The controller is placed outside the instrumentation room to reduce potential interference.

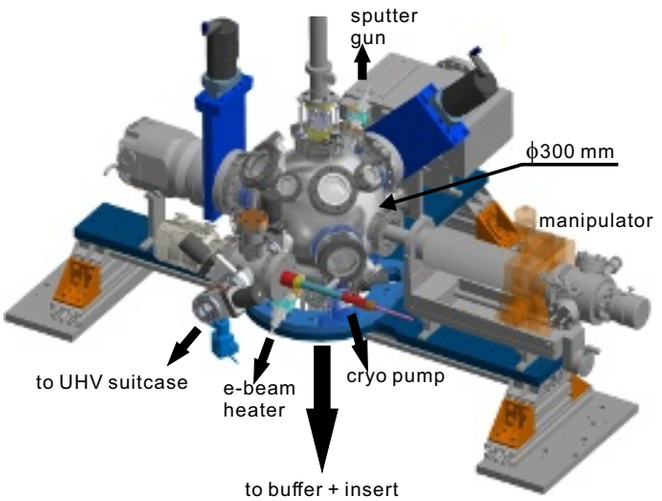

FIG. 2. Sketch of the UHV chambers consisting of a spherical preparation chamber with a diameter of 300 mm and a loadlock. The preparation chamber is equipped with a sputter gun, an e-beam heater, and a three-axis manipulator. A UHV suitcase can be docked to the loadlock which is pumped by a turbo pump and a home built cryo-pump.

III. UHV ASSEMBLY

To study the intrinsic properties of materials by STM, it is important that the surface does not experience heavy contamination, and our facility consisting of a loadlock, a preparation chamber, and a cryogenic insert is therefore designed to be fully UHV compatible (see Fig. 2). The whole facility is rigidly mounted on the aluminium table. The loadlock is designed in such a way that a portable UHV suitcase containing thin films from our oxide thin-film lab can be docked via a gate valve. It is equipped with a turbo molecular pump and a home-built cryo-pump by cooling active charcoal with liquid helium. Our test of the efficiency of the cryo-pump shows that the pressure can be lowered by a factor of $3 \sim 5$ in 10 min (reduced from 1×10^{-8} mbar to the lower range of 10^{-9} mbar). In this way the total time for getting the pressure in the loadlock to the lower range of 10^{-9} mbar from ambient condition is less than 6 hours, during which the thin film sample can be sitting in a vacuum $< 1 \times 10^{-9}$ mbar in the transfer suitcase.

The preparation chamber is spherical and equipped with a few standard surface preparation techniques including an e-beam heater, an ion source sputtering gun, a manipulator

with both heating/cooling stages, and a cleaving stage. It is prepared for evaporators for e.g. thin film deposition or tip coating for spin-polarized measurements [4]. With these equipments pristine samples and STM tips of high quality can be prepared *in vacuo*. The cross transfer of sample/tip between the loadlock and preparation chamber is done with the manipulator and a transfer rod in the suitcase.

The bottom of the preparation chamber is connected to a buffer UHV tube via a first gate valve, which is then connected to the cryogenic insert via a second gate valve. We gain two advantages from such a design. Firstly, the insert containing the STM can be detached from the top chamber for extremely low noise measurement. Secondly, the insert can be separately baked out. A non-evaporable getter pump (SAES Group) is mounted at the buffer tube to efficiently pump the commonly known residual hydrogen at the cryogenic insert [31, 32]. The sample/tip transfer between the preparation chamber and STM is accomplished by a two-meter long vertical transfer rod.

IV. STM HEAD AND CRYOGENIC INSERT

The microscope head is built based on the design by Hanaguri *et al* [33]. For STM working at a low temperature, high stiffness and rapid thermalization are highly demanded. To this end, we adopted the so called Pan-design motor as the coarse approach mechanism, which is driven by six shear piezo stacks [34]. Further care has been taken for choice of the building materials. The head is bolted to a hexagonal Cu-Be plate which is in the meantime used as the sample receptacle. Sample is glued to a Cu-Be holder and then screwed into the receptacle. The upper (lower) panel of Fig.3**(a)** shows a photo of the head without (with) the sample receptacle. In STM experiments tips made of different materials, such as Pt/Ir, W, Cr, or Nb, treated *in vacuo* with e.g. ion sputtering and e-beam bombardment can be utilized to realize special purposes such as spin-polarized imaging or high energy resolution measurement [35–37]. Therefore, an *in-situ* tip exchange mechanism is equipped without sacrificing the performance of the setup [33].

The whole STM unit is rigidly attached to a plate cooled by the 1 K cooling system in the cryogenic insert (see Fig.3**(b)**), that is placed in the liquid helium dewar housing the vector

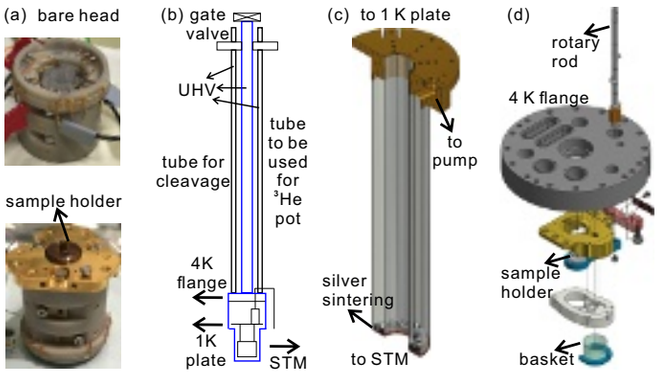

FIG. 3. Cryogenic insert. **(a)** Photos of the bare head (upper panel) and the head with a sample (lower panel). The head is bolted to a hexagonal Cu-Be sample receptacle. The sample is glued to a Cu-Be holder that is screwed into the receptacle. **(b)** schematic showing the STM insert. The blue area is UHV compatible. The top gate valve is connected to a buffer UHV tube which is further connected to the preparation chamber. The STM is thermally connected to the 1 K plate and located at the center of the vector magnetic field. **(c)** A home-designed ^{3}He pot to be used to update the refrigerator. **(d)** A home-built *in situ* cleaving stage directly mounted on the 4 K flange. The sample holder is screwed into the 4K sample-receptacle (blue). The cleavage is realized through the rotary movement of the rod using a mechanical feedthrough at the top flange of the insert (not shown here).

magnet assembly. In addition, a heater is mounted on the 1 K plate allowing for variable temperature up to ~ 300 K. One unique feature of our insert is that the refrigerator can be easily updated with a home-built ^{3}He pot so that a sub-Kelvin base temperature can be reached. Fig.3**(c)** shows our design of the ^{3}He pot to be attached to the 1 K plate.

Surfaces of some materials can undergo reconstruction upon cleavage. In order to study intrinsic properties of such materials by STM, low temperature cleavage is inevitably required. We therefore built a cleaving stage attached to the insert which is thermally anchored to the flange held at 4.2 K (shown in Fig.3**(d)**). In order to cleave a sample, a nonmagnetic metal stick is glued normal to the sample surface. Then the sample holder is screwed into the 4K sample-receptacle (blue in Fig.3**(d)**), which is fixed on a rotary rod controlled by a mechanical feedthrough. After sufficient time for thermalization, quickly rotating the feedthrough causes the sample to move towards the wall of a metal block (silver in Fig.3(d)) to kick off

the metal stick. A basket is located immediately below the stage to collect the falling parts. In addition, the stage can also be used to pre-cool warm samples before being inserted into the microscope head as well as to store samples for months without suffering from residual gas contamination by utilizing the cryogenic vacuum on the order of 10^{-12} mbar.

V. ROTATABLE DEWAR

Our cryostat supplied by ICE Oxford [38] is of top-loading design. It utilizes super-insulation instead of liquid nitrogen for thermal insulation, thus preventing the well-known vibration noise induced by liquid-nitrogen boil-off. It has a liquid helium reservior of $\sim 90\,$l, of which $\sim 65\,$l is above the capillary pickup of the 1 K cooling system and the vector magnet assembly. The average boil-off rate is $\sim 9\,$l/day, and therefore our facility can run continuously at the base temperature for ~ 7 days. Such a long holding time allows us to carry out time-consuming experiments such as quasiparticle interference mapping by spectroscopic-imaging STM [14].

The vector magnet assembly, manufactured by Cryomagnetics, Inc. [39], is submerged directly in the liquid helium reservoir and held at 4.2 K. It consists of one solenoid coil magnet (B_z, red in Fig.4**(a)**) in the vertical direction and one split-pair coil magnet (B_x, blue in Fig.4**(a)**) in the horizontal direction; the direction is defined with respect to the sample surface located at the center of the bore (see Fig.4**(a)**). With them, fields of up to 9 T and 3 T can be applied for B_z and B_x, respectively. To achieve a vector field B_r, firstly B_z and B_x are simultaneously applied, resulting in a field of up to 3 T in any direction on a vertical circular orbit; the ratio of B_z and B_x determines the polar angle θ of the field. Then the dewar is mechanically rotated about the cryogenic insert (the black arrow in Fig.4**(a)**), to change the azimuthal angle ϕ. In this way we obtain a field B_r of up to 3 T in any direction as described by the polar and azimuthal angles between the field and sample surface (θ, ϕ). In order to determine the exact θ and ϕ, we firstly extract from the design the orientation of the microscope relative to the magnets after rotation. We then record an atomically resolved topographic image and extract the orientation of the sample surface relative to the microscope. These allow us to calculate the angle in-plane alignment with a precision better than 1°. The polar angle is determined by the nominal applied fields with

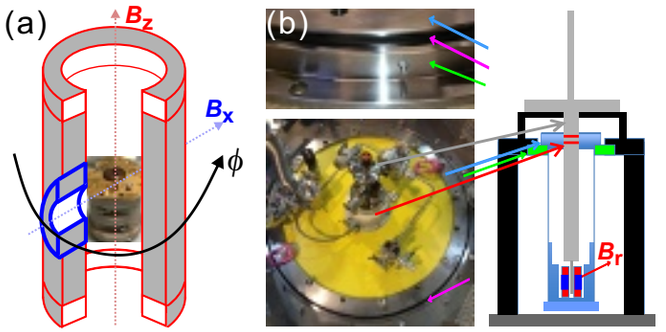

FIG. 4. **(a)** Schematics showing the principle how a vector field B_r of up to 3 T in any direction can be applied to the sample located at the center of the magnet bore. The solenoid coil (red) and the split-pair coil (blue), that are mechanically anchored at the dewar bottom, generate B_z and B_x perpendicular to and along the sample surface, respectively. The superposition of B_z and B_x yields the total vector field $B_r(\theta, \phi)$. The azimuthal angle ϕ can be changed by rotating the dewar relative to the cryogenic insert (z axis) using a rotatable bearing as shown in **b**. The photo shows our STM head. **(b)** (Left panel) Side- and top-view photos of the rotatable bearing installed at the dewar neck. The outer (green arrows) and inner (blue arrows) races are respectively bolted to the aluminium table and dewar. Additionally, viton rings are used between the dewar and out race (violet arrows), and the dewar and insert (red arrow), the latter so called double viton-ring sliding seal tightly sealing the liquid helium in the dewar. (Right panel) Schematics of the whole facility showing the position of the bearing. The vector magnet (in red and blue, B_r) is bolted at the dewar bottom and is therefore rotated along with the dewar with respect to the cryogenic insert. The double viton-ring sliding seal between the dewar and insert is shown with two red lines (red arrow).

accuracy limited by magnet hysteresis. With this knowledge, we finally compute the angles θ and ϕ based on the magnitude of the applied fields.

The rotation of the field azimuthal direction is realized by turning the dewar about the axis of the insert using a viton seal and a bearing, instead of turning the insert as done by others [26]. As shown in Fig. 4**(b)**, in order to rotate the dewar while keeping it sealed, we employ a double viton-ring sliding seal to couple the dewar and insert, as used in many other circumstance e.g. in rotating-insert setups. Our seal has been tested to be helium

tight using a leak detector. The bearing assembly is mounted with the outer and inner races bolted to the aluminium table and dewar, respectively (see Fig. 4**(b)**). An additional viton ring is used between the dewar and outer race. Because the outer race, the UHV chambers and therefore, the insert are rigidly bolted to the aluminium table, their relative geometrical configuration remains unchanged. In this way turning the dewar (and therefore the magnets) relative to the outer race results in the change of the field direction relative to the insert housing the microscope. The use of viton rings in our design for the rotation mechanism is found to efficiently damp the mechanical vibration transmitted to the microscope from the dewar rotation, thus protecting the tunneling junction of the sample and tip. Comparing to the use of a rotatable insert as reported in e.g. [23, 26], two advantages are gained with our strategy. Firstly, because the insert is not required to turn while maintaining the field of view with movements $< 10\,\mathrm{nm/T}$, it can be kept rigidly connected to the upper chamber making the fully UHV compatible design possible. Secondly, because the insert containing the STM assembly is not touched at all during operation, the tunneling junction in the insert is protected from any potential mechanical shock over the whole operation period and consequently the tip and scanning area remain undisturbed.

VI. PERFORMANCE

To demonstrate that the facility is operational and meets the design criteria, we carried out experiments on samples with atomically flat and clean surfaces. While thin films were transferred via the UHV suitcase, all layered bulk samples were cleaved at the cleaving stage at 4.2 K and then immediately inserted into the microscope head. The tips were electrochemically etched from a W wire and cleaned by e-beam bombardment in the preparation chamber to remove oxide layers at the apex, followed by *in situ* conditioning on the Cu(111) surface with field emission. Fig.5**(a)** shows an atomically resolved topography of semimetallic Fe_3Sn_2 imaged at zero field. A well-ordered honeycomb lattice with a few vacancy and adatom defects is clearly visible, as previously reported by other groups [40, 41]. The inset of Fig.5**(a)** displays the height profile along the blue dashed line across an adatom defect as shown in the main panel. It is immediately seen that the vertical z noise level is less than 0.5 pm thus proving the high stability of our setup. The power spectrum of tunneling current shows that the noise is below $20\,\mathrm{fA}/\sqrt{Hz}$ and the band RMS noise ranging from 0

to 1000 Hz is less than 0.35 pA. These noise levels are comparable to the ones at ultra low noise facilities reported by other groups [26, 42].

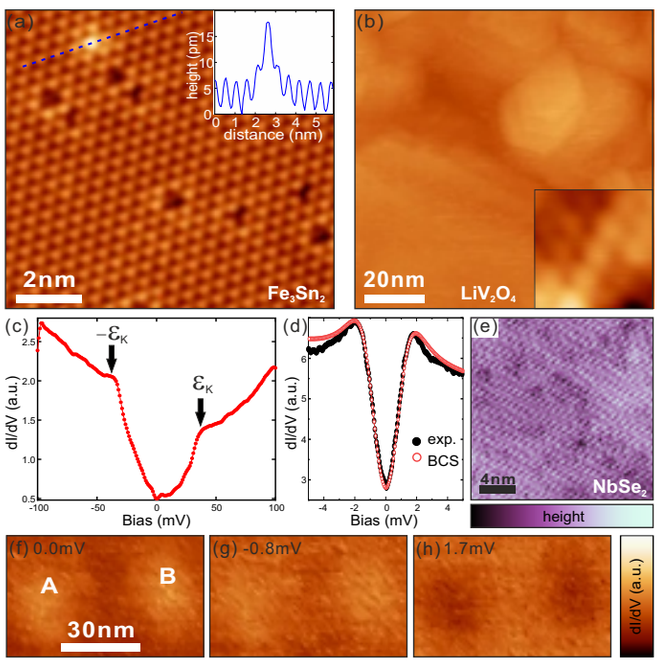

FIG. 5. **(a)** Topography of Fe_3Sn_2 at 500 mV. Adatom and vacancy defects are visible as white and black features, respectively. Inset shows a profile along the blue dashed line over an adatom defect. **(b)** Topography of LiV_2O_4 thin film at 1000 mV. Inset shows topography at 400 mV (size: 1.3 nm $\times$ 1.3 nm.). **(c)** A dI/dV curve over a large energy range resolving kink features $\pm\varepsilon_K$ related with the CDW phase in 2 H$-$$NbSe_2$. **(d)** A d$I$/d$V$ curve along with a fit to BCS theory (see text) over a small energy range resolving the superconducting phase in 2 H$-$$NbSe_2$. **(e)** Topography of 2 H$-$$NbSe_2$ at -50 mV resolving the CDW phase. **(f-h)** Differential conductance dI/dV maps of 2 H$-$$NbSe_2$ at different energies as labeled, with $B_z = 0.5$ T and $B_x = 2.0$ T simultaneously applied to the surface. All data were recorded at $T = 4.2$ K.

Fig.5**(b)** shows a typical topography of a LiV_2O_4 thin film deposited on $SrTiO_3$(111) by pulsed laser deposition (PLD) in our oxide thin-film lab. It was transferred with the UHV suitcase and further heated in the preparation chamber. Atomically flat and clean hexagonal islands of LiV_2O_4(111) are clearly seen. The inset shows an area with atomic resolution. Thus, it proves the capability of our facility for the local-probe study of complex

heterostructures grown by a separate thin-film growth setup.

To demonstrate the spectroscopy capability, we measured well characterized 2 H−$NbSe_2$ which hosts coexisting charge density wave (CDW) and superconducting phases at the temperature below $\sim$ 7 K. Fig.5**(c)** displays a differential conductance curve dI/d$V(V)$ over a large energy range from -100 mV to 100 mV. Suppression in the spectral weight around the Fermi level (E_f) is clearly resolved. In addition, two features $\pm\varepsilon_K$ at about $\pm$35 mV are revealed. Such kink features have been reported by other groups and discussed to be intimately related with the CDW phase [43, 44]. The well-known 3×3 CDW pattern in real space can be clearly imaged in the topography mode with atomic resolution, as shown in Fig.5**(e)**. In Fig.5**(d)** we present a high resolution spectroscopic curve from -5 mV to 5 mV (black). We can see that the experimental curve resolves the fine spectral depression between -2 mV and 2 mV near E_f which can be unambiguously ascribed to the superconducting energy gap in 2 H−$NbSe_2$. The signal-to-noise ratio is comparable to a similar facility without a vector magnet running also in the Precision Laboratory at Max Planck Institute in Stuttgart [45]. While a perfect fit to the conventional BCS theory is not possible because the superconductivity of 2 H−$NbSe_2$ is anisotropic, we nevertheless perform simulation within the BCS framework by assuming a gap of $\sim$ 1.0 meV and linear weak background to capture the slight asymmetry in the lineshape with respect to E_f, shown in red.

We utilize the superconductivity of 2 H−$NbSe_2$ to demonstrate its spectroscopic-imaging capability in rotating magnetic fields. Fields of $B_z = 0.5$ T and $B_x = 2.0$ T were simultaneously applied to the surface to induce electronic inhomogeneity, and spectroscopic curves ranging from -2.0 mV to 2.0 mV with 0.1 mV interval were recorded over a field of view of 150 nm $\times$ 125 nm (304 $\times$ 254 pixels). Typical dI/dV maps are displayed in Fig.5**(f-h)** for selected energies of 0.0 mV, -0.8 mV, and 1.7 mV, respectively. Two vortices are clearly visible as bright areas in Fig.5**(f)**, marked as A and B, reflecting the suppression of superconductivity at the cores. When the energy is moved closer to the coherence peak i.e. at 1.7 mV (see Fig.5**(d)**), the contrast is reversed (Fig.5**(h)**). At -0.8 mV (Fig.5**(g)**) the contrast becomes hardly visible, suggesting it corresponding to the crossover energy.

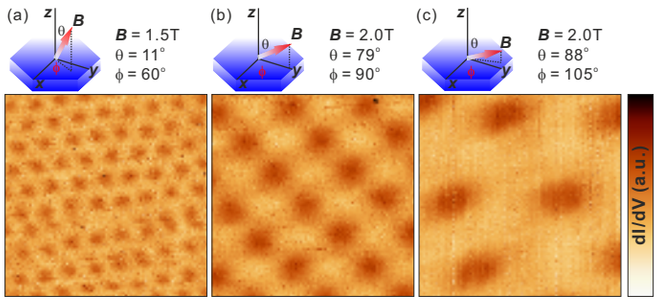

FIG. 6. Differential conductance $\mathrm{d}I/\mathrm{d}V$ maps of 2 H−$NbSe_2$ in magnetic fields of **(a)** $B = 1.5\,\mathrm{T}$ along ($\theta = 11°$, $\phi = 60°$), **(b)** $B = 2.0\,\mathrm{T}$ along ($\theta = 79°$, $\phi = 90°$), and **(c)** $B = 2.0\,\mathrm{T}$ along ($\theta = 88°$, $\phi = 105°$). The field of view is 300 nm × 300 nm. All data were recorded at a bias of 0.3 mV and $T = 4.2\,\mathrm{K}$.

Because 2 H−$NbSe_2$ is a layered type-II superconductor at the temperature below $\sim 7\,\mathrm{K}$, it is an excellent platform to calibrate a magnetic field by imaging the vortex lattice, as shown above (see Fig.5**(f-h)**). It has been found that two instabilities in the vortex structure set in when the applied magnetic field is tilted greater than $\sim 80°$ from the normal direction, which can be imaged by STM [46]. Therefore, the vortex lattice can be exploited to demonstrate the performance of the vector magnet by mapping its evolution with rotating the field direction. The vector field is achieved by combining rotating the dewar and applying the perpendicular field simultaneously with the in-plane one, as described in the previous section. In this demonstration experiment we apply a field of up to 2 T with different θ and ϕ relative to the sample surface. Because the magnetic field can potentially induce strain due to e.g. magnetostriction in the building materials which could lead to a tip drift or even crash into the sample, over this period the tip is retracted from tunneling contact by $\sim 250\,\mathrm{nm}$. We find that the tip-sample lateral position changes between each rotation of the 2 T field by less than 20 nm corresponding to a maximum drift rate $< 20\,\mathrm{nm}/2\,\mathrm{T} = 10\,\mathrm{nm/T}$ assuming linear magnetostriction as the primary source of the movement. The key importance of this figure of merit is the capability to measure the same atomic area of the sample after rotation. While our drift is seemingly slightly larger than that achieved by Trainer *et al* [26], both are more than sufficient for the scientific plans, given that the maximum scanning field-of-view 1500 nm×1500 nm of our tube scanner is orders of magnitude larger than the drift. Fig.6**(a-c)** display a series of $\mathrm{d}I/\mathrm{d}V$ maps showing distinct vortex lattices, taken at the bias of $V_b = 0.3\,\mathrm{mV}$ between the superconducting coherence peaks (see Fig.5**(d)**), in the presence

of the field. Clearly, the response of the vortex lattice to the applied field significantly depends on the field inclination. When the field is almost perpendicular to the surface (the polar angle $\theta = 11°$ and azimuth angle $\phi = 60°$), a well-known regular hexagonal lattice is formed (Fig.6**(a)**). The vortex spacing $s = 37.0\,\mathrm{nm}$ agrees very well with the theoretical value 36.2 nm expected from the formula

$$s = \sqrt{\frac{\sqrt{3}\Phi_0}{2B}} \tag{1}$$

with Φ_0 and B being the magnetic flux quantum and magnetic field, respectively. When the field is tilted from the normal direction and towards the in-plane direction, the flux lattice is deformed. At the polar angle $\theta = 79°$ and azimuth angle $\phi = 90°$ achieved by applying the perpendicular field simultaneously with the in-plane one, ordered rows of vortices are observed as seen in Fig.6**(b)**. Although the field strength is higher, the lattice spacing is much larger as compared with that in Fig.6**(a)**. In addition, the vortex lattice is more rectangular shaped. As the polar angle θ further increases while maintaining the field strength constant, not only the lattice becomes strongly disordered, but also the individual vortex core is elongated resulting in a comet shaped structure with streak features weakly visible, as shown in Fig.6**(c)** for $\theta = 88°$ and $\phi = 105°$. Note that this configuration was achieved from that of Fig.6**(b)** by solely rotating the dewar with respect to the insert, because our sample surface was not perfectly perpendicular to the insert axis. Our observations nicely reflect the strong anisotropy in the superconductivity of $2\,\mathrm{H}-\mathrm{NbSe_2}$ and are consistent with the reported results [46]. We would like to stress that over the whole period of rotating the dewar, we observed only a slight movement $< 10\,\mathrm{nm/T}$ in the scanning area and no change in the tip.

VII. CONCLUSION

To summarize, we have designed and built a fully UHV compatible spectroscopic-imaging STM working in a vector magnet of up to 9 T and 3 T in the perpendicular and any other direction, respectively, at a variable temperature from $\sim$ 300 K down to $\sim$ 1.5 K. High stability and resolution of topography and spectroscopy modes have been demonstrated on samples cleaved at the liquid helium temperature in UHV condition and on thin film samples transferred from a separate facility. The operation of the vector magnet has been tested with

the tip and scanning area being undamaged benefiting from the rigidity of our STM head and rotating the dewar only. The capabilities of our facility open up the possibility of STM investigation of quantum materials in a large parameter space, such as the study of nontrivial spin textured band structures and field-induced unconventional superconductivity in layered compounds and artificial thin films grown in external MBE and PLD facilities [40, 47].

VIII. ACKNOWLEDGMENTS

The work has been supported by the Alexander von Humboldt foundation. A.W.R. acknowledges support by EPSRC grant EP/P024564/1. We thank M. Dueller, K. Pflaum, I. Pentegov, and ICE Oxford for valuable technical assistance. We also thank T. Hanaguri and J.C. Davis for stimulating discussion. Fe_3Sn_2 samples were supplied by L. Prodan, V. Tsurkan, and Istvan Kezsmarki, University of Augsburg. The LiV_2O_4 thin film was grown in collaboration with Tim Schweizer and Dennis Huang.

IX. AUTHOR DECLARATIONS

A. Conflict of Interest

The authors have no conflicts to disclose.

X. DATA AVAILABILITY

The data that support the findings of this study are available from the corresponding author upon reasonable request.

[1] G. Binnig, H. Rohrer, Ch. Gerber, and E. Weibel, Phys. Rev. Lett. **49**(1), 57 (1982).

[2] G. Binnig and H. Rohrer, Rev. Mod. Phys. **59**(3), 615 (1987).

[3] H. F. Hess, R. B. Robinson, R. C. Dynes, J. M. Valles, and J. V. Waszczak, Phys. Rev. Lett. **62**(2), 214 (1989).

[4] R. Wiesendanger, Rev. Mod. Phys. **81**(4), 1495 (2009).

[5] Ø. Fischer, M. Kugler, I. Maggio-Aprile, C. Berthod, and C. Renner, Rev. Mod. Phys. **79**(1), 353 (2007).

[6] A. Yazdani, E. H. da Silva Neto, and P. Aynajian, Annual Review of Condensed Matter Physics **7**(1), 11 (2016).

[7] K. Bian, C. Gerber, A. J. Heinrich, D. J. Müller, S. Scheuring, and Y. Jiang, Nature Reviews Methods Primers **1**(1), 36 (2021).

[8] J.-X. Yin, S. H. Pan, and M. Z. Hasan, Nature Reviews Physics **3**(4), 249 (2021).

[9] B. Jäck, Y. Xie, and A. Yazdani, Nature Reviews Physics **3**, 541 (2021).

[10] C. F. Hirjibehedin, C. P. Lutz, and A. J. Heinrich, Science **312** (5776), 1021 (2006).

[11] L. Zhou, J. Wiebe, S. Lounis, E. Vedmedenko, F. Meier, S. Blügel, P. H. Dederichs, and R. Wiesendanger, Nature Physics **6**(3), 187 (2010).

[12] S. Nadj-Perge, I. K. Drozdov, J. Li, H. Chen, S. Jeon, J. Seo, A. H. MacDonald, B. Andrei Bernevig, and A. Yazdani, Science **346**(6209), 602 (2014).

[13] L. Cornils, A. Kamlapure, L. Zhou, S. Pradhan, A. A. Khajetoorians, J. Fransson, J. Wiebe, and R. Wiesendanger, Phys. Rev. Lett. **119**(19), 197002 (2017).

[14] J. E. Hoffman, E. W. Hudson, K. M. Lang, V. Madhavan, H. Eisaki, S. Uchida, and J. C. Davis, Science **295**(5554), 466 (2002).

[15] M. Z. Hasan and C. L. Kane, Rev. Mod. Phys. **82**(4), 3045 (2010).

[16] X.-L. Qi and S.-C. Zhang, Rev. Mod. Phys. **83**(4), 1057 (2011).

[17] B. Yan and C. Felser, Annual Review of Condensed Matter Physics **8**(1), 337 (2017).

[18] N. P. Armitage, E. J. Mele, and A. Vishwanath, Rev. Mod. Phys. **90**(1), 015001 (2018).

[19] B. Q. Lv, T. Qian, and H. Ding, Rev. Mod. Phys. **93**(2), 025002 (2021).

[20] A. Manchon, H. .C. Koo, J. Nitta, S. M. Frolov, and R. A. Duine, Nature Materials **14**(9), 871 (2015).

[21] R. Wiesendanger, Nature Reviews Materials **1**(7), 16044 (2016).

[22] A. Fert, N. Reyren, and V. Cros, Nature Reviews Materials **2**(7), 17031 (2017).

[23] W. Cai, F. Pang, J. Wang, H. Liu, X. J. Liang, Q. K. Xue, and D. M. Chen, Review of Scientific Instruments **78**(6), 065108 (2007).

[24] S. Meckler, M. Gyamfi, O. Pietzsch, R. Wiesendanger, Review of Scientific Instruments **80**(2), 023708 (2009).

[25] J. A. Galvis, E. Herrera, I. Guillamón, J. Azpeitia, R. F. Luccas, C. Munuera, M. Cuenca, J. A. Higuera, N. Díaz, M. Pazos, M. García-Hernandez, A. Buendía, S. Vieira, and H. Suderow, Review of Scientific Instruments **86**(1), 013706 (2015).

[26] C. Trainer, C. M. Yim, M. McLaren, and P. Wahl, Review of Scientific Instruments **88**(9), 093705 (2017).

[27] H. von Allwörden, A. Eich, E. J. Knol, J. Hermenau, A. Sonntag, J. W. Gerritsen, D. Wegner, and A. A. Khajetoorians, Review of Scientific Instruments **89**(3), 033902 (2018).

[28] F. D. Natterer, F. Patthey, T. Bilgeri, P. R. Forrester, N. Weiss, H. Brune, Review of Scientific Instruments **90**(1), 013706 (2019).

[29] D. Wong, S. Jeon, K. P. Nuckolls, M. Oh, S. C. J. Kingsley, and A. Yazdani, Review of Scientific Instruments **91**(2), 023703 (2020).

[30] To the best of our knowledge, the product USM1300 from Unisoku (Japan) has a vector field of 9 T/2 T/2 T configuration and is the only one that can apply a 3D field above 1 T in any direction.

[31] F. D. Natterer, F. Patthey, and H. Brune, Surface Science **615**, 80 (2013).

[32] Q. Dubout, F. Donati, C. Wäckerlin, F. Calleja, M. Etzkorn, A. Lehnert, L. Claude, P. Gambardella, and H. Brune, Phys. Rev. Lett. **114**(10), 106807 (2015).

[33] T. Hanaguri, Journal of Physics: Conference Series **51**, 514 (2006).

[34] S. H. Pan, International Patent Publication No. WO 93/19494 (International Bureau, World Intellectual Property Organization), September 30, 1993.

[35] L. Zhou, F. Meier, J. Wiebe, R. Wiesendanger, Phys. Rev. B **82**(1), 012409 (2010).

[36] P. Löptien, L. Zhou, A. A. Khajetoorians, J. Wiebe, and R. Wiesendanger, Journal of Physics: Condensed Matter **26**(42), 425703 (2014).

[37] P. Löptien, L. Zhou, A. A. Khajetoorians, J. Wiebe, and R. Wiesendanger, Surface Science **643**, 6 (2016).

[38] ICE Oxford Ltd, Ave Four, Witney OX28 4BN, UK.

[39] Cryomagnetics Inc., Oak Ridge, TN.

[40] J.-X. Yin, S. S. Zhang, H. Li, K. Jiang, G. Chang, B. Zhang, B. Lian, C. Xiang, I. Belopolski, H. Zheng, T. A. Cochran, S. Y. Xu, G. Bian, K. Liu, T. R. Chang, H. Lin, Z. Y. Lu, Z. Wang, S. Jia, W. Wang, M. Zahid Hasan, Nature **562**(7725), 91 (2018).

[41] Z. Lin, J.-H. Choi, Q. Zhang, W. Qin, S. Yi, P. Wang, L. Li, Y. Wang, H. Zhang, Z. Sun, L. Wei, S. Zhang, T. Guo, Q. Lu, J.-H. Cho, C. Zeng, and Z. Zhang, Phys. Rev. Lett. **121**(9), 096401 (2018).

[42] L. Zhang, T. Miyamachi, T. Tomanić, R. Dehm, and W. Wulfhekel, Review of Scientific Instruments **82**(10), 103702 (2011).

[43] H. F. Hess, R. B. Robinson, and J. V. Waszczak, Physica B: Condensed Matter **169**(1), 422 (1991).

[44] A. Soumyanarayanan, M. M. Yee, Y. He, J. van Wezel, D. J. Rahn, K. Rossnagel, E. W. Hudson, M. R. Norman, and J. E. Hoffman, Proceedings of the National Academy of Sciences **110**(5), 1623 (2013).

[45] Markus Ternes, private communications.

[46] H. F. Hess, C. A. Murray, and J. V. Waszczak, Phys. Rev. Lett. **69**(14), 2138 (1992).

[47] K. Yang and D. F. Agterberg, Phys. Rev. Lett. **84**(21), 4970 (2000).

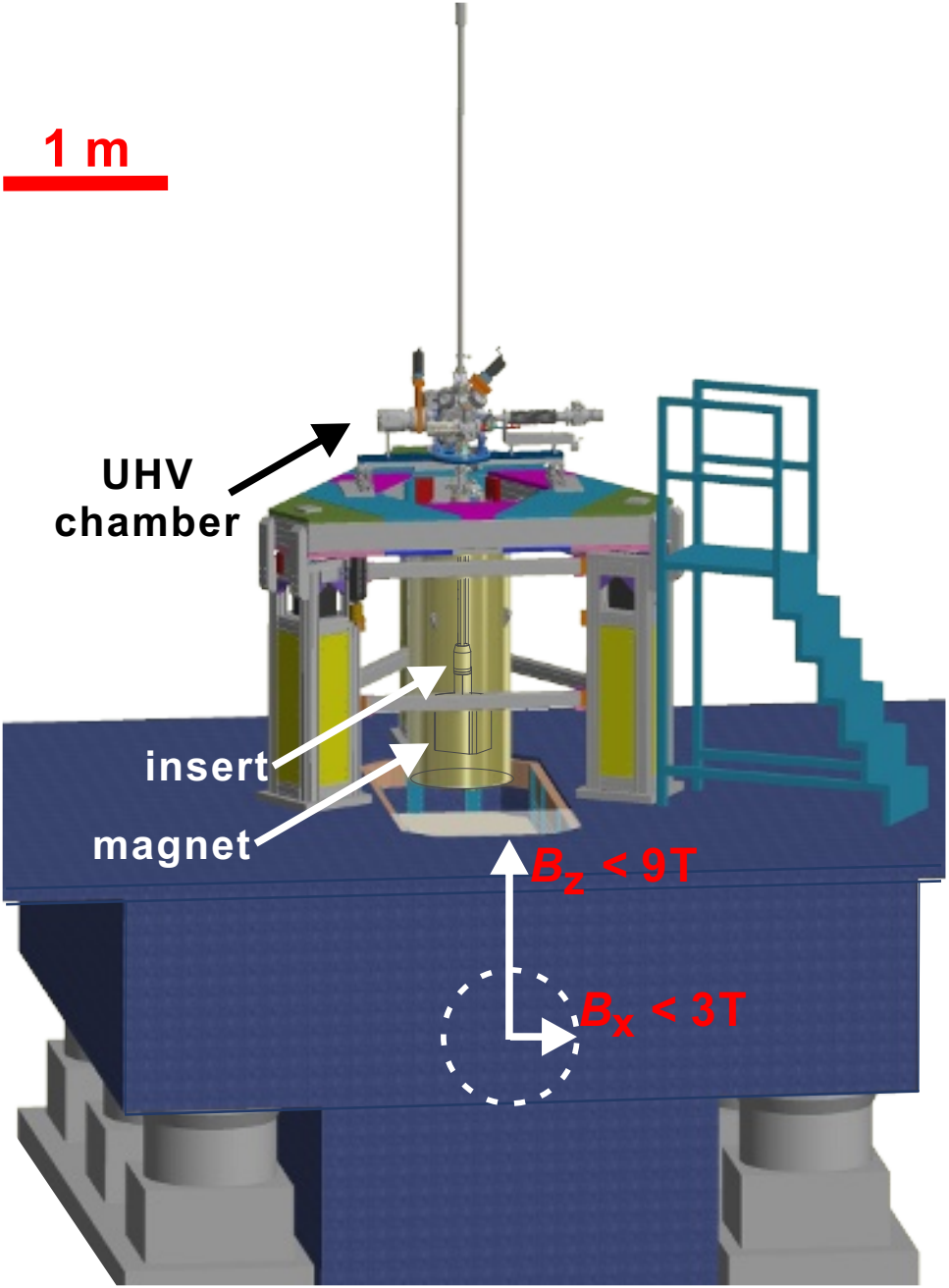

-- instrument:
chamber
insert
cryostat

-- table

-- damper

-- concrete floor

-- damper

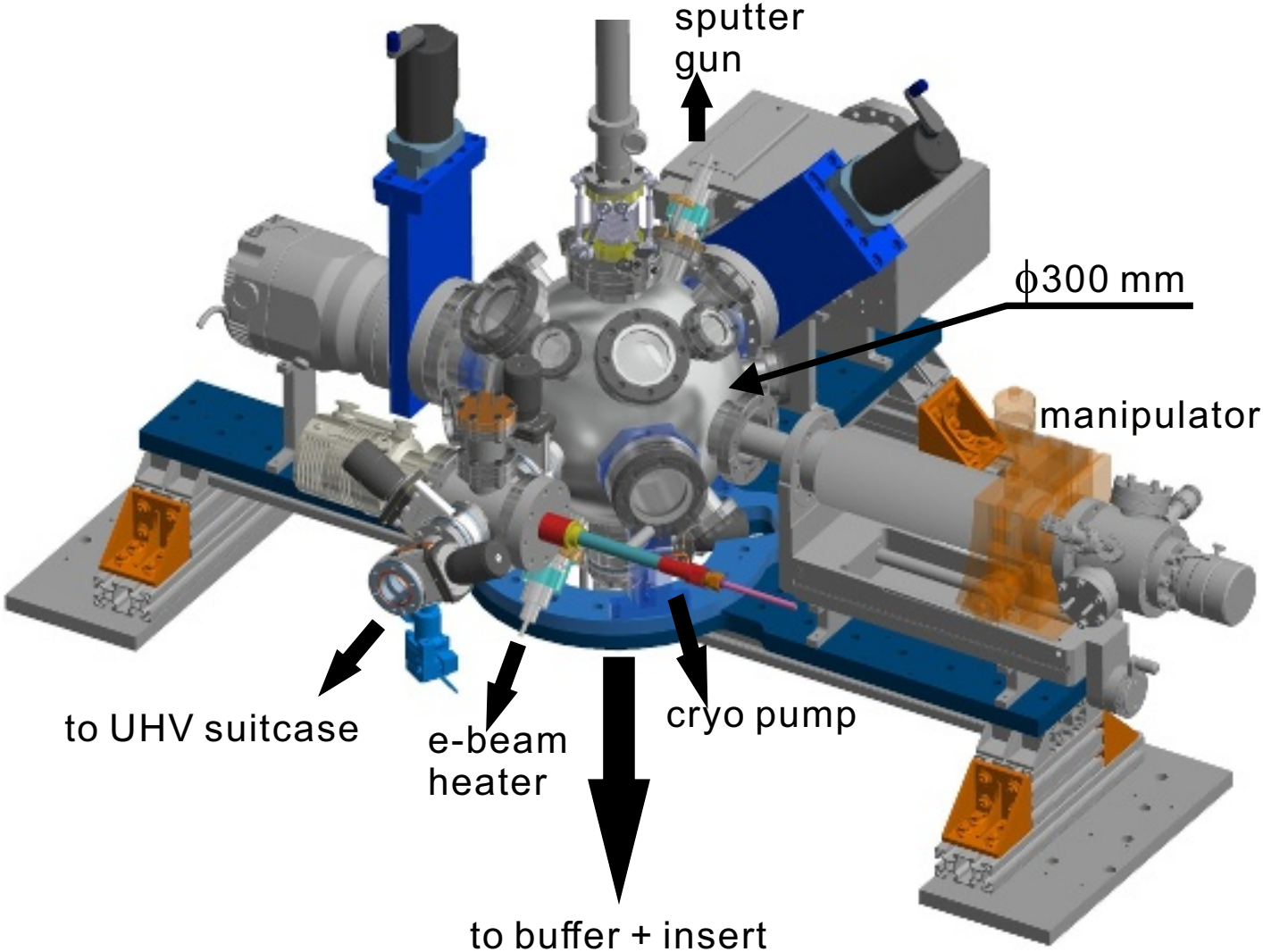
sputter
gun
ϕ300 mm
manipulator
to UHV suitcase
e-beam
heater
cryo pump
to buffer + insert

(a) bare head

sample holder

(b) gate valve

UHV

tube for cleavage

tube to be used for ^{3}He pot

4K flange

1K plate

STM

(c) to 1 K plate

to pump

silver sintering

to STM

(d)

rotary rod

4 K flange

sample holder

basket

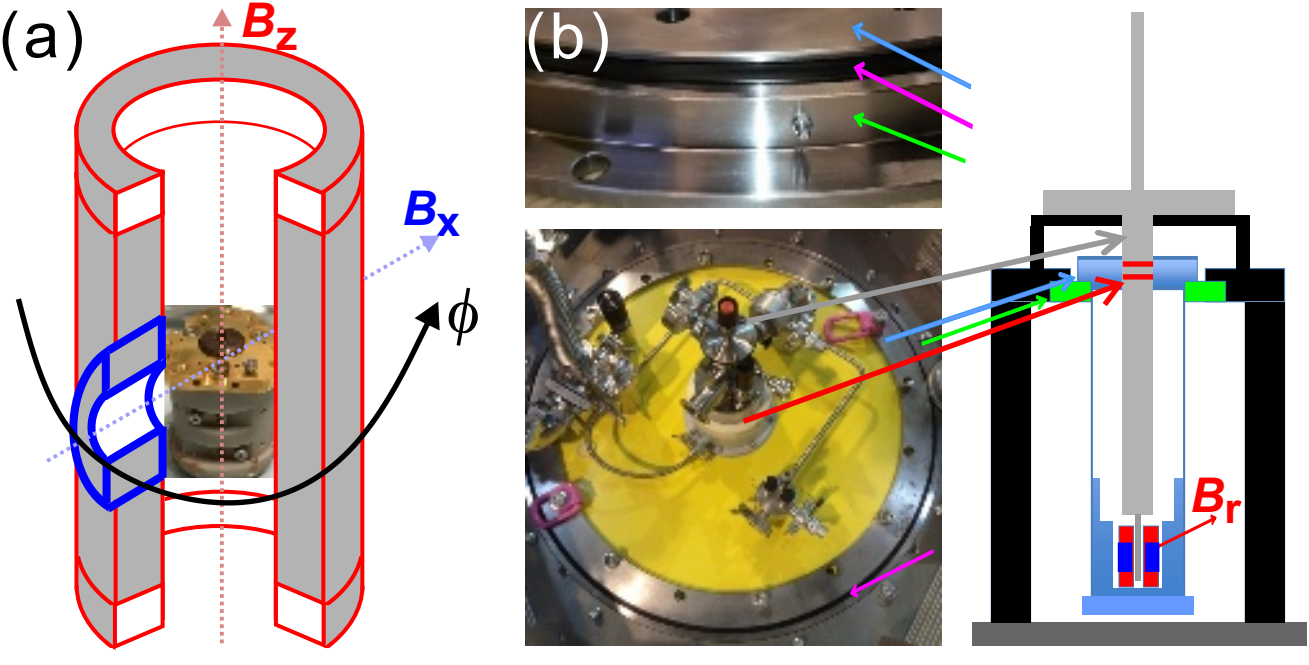
(a)
B_z
B_x
ϕ
(b)
B_r

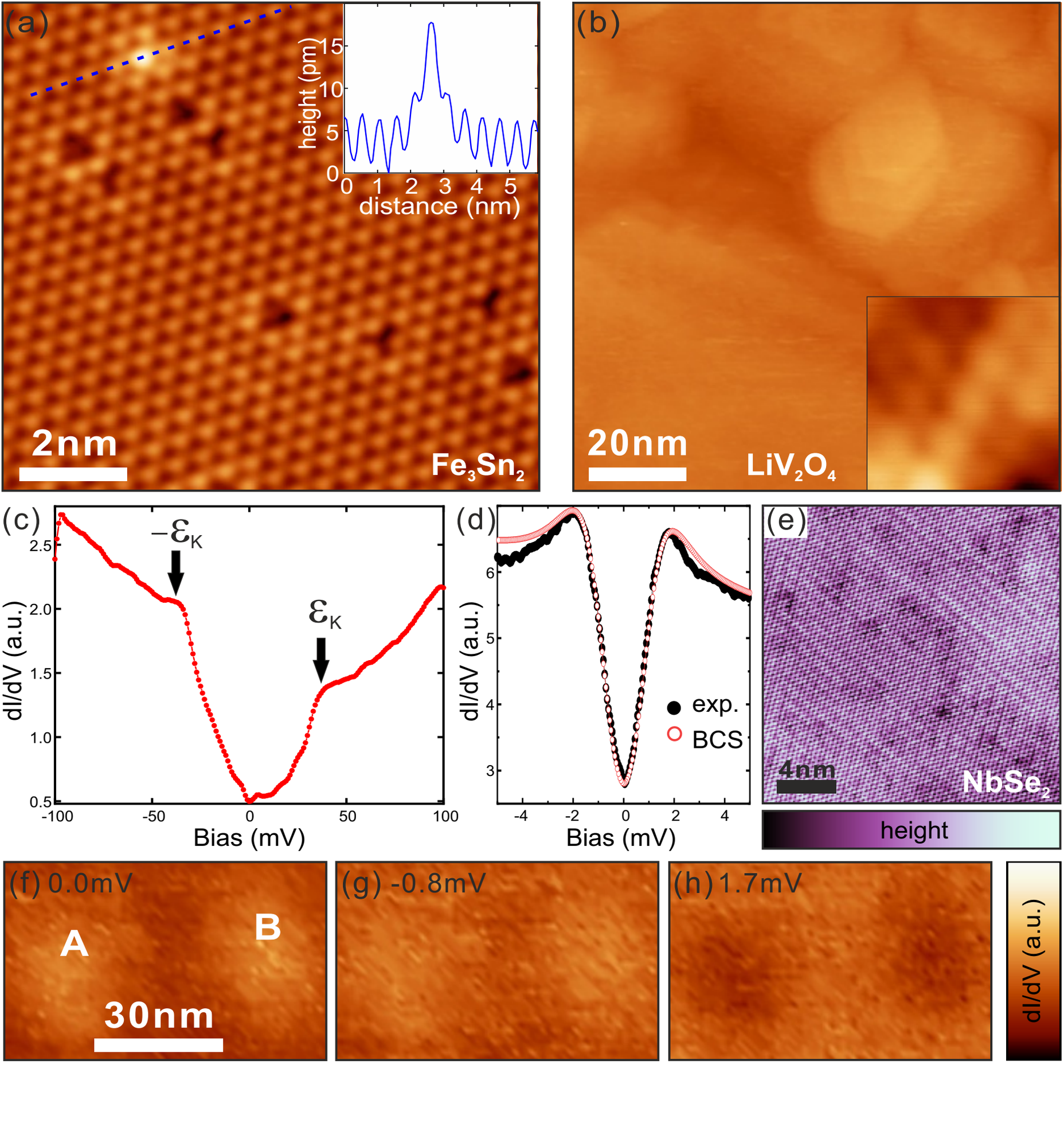
(a)
height (pm)
15
10
5
0
0 1 2 3 4 5
distance (nm)
2nm
Fe3Sn2
(b)
20nm
LiV2O4
(c)
−εK
εK
dI/dV (a.u.)
2.5
2.0
1.5
1.0
0.5
-100 -50 0 50 100
Bias (mV)
(d)
dI/dV (a.u.)
6
5
4
3
exp.
BCS
-4 -2 0 2 4
Bias (mV)
(e)
4nm
NbSe2
height
(f) 0.0mV
A
B
30nm
(g) -0.8mV
(h) 1.7mV
dI/dV (a.u.)

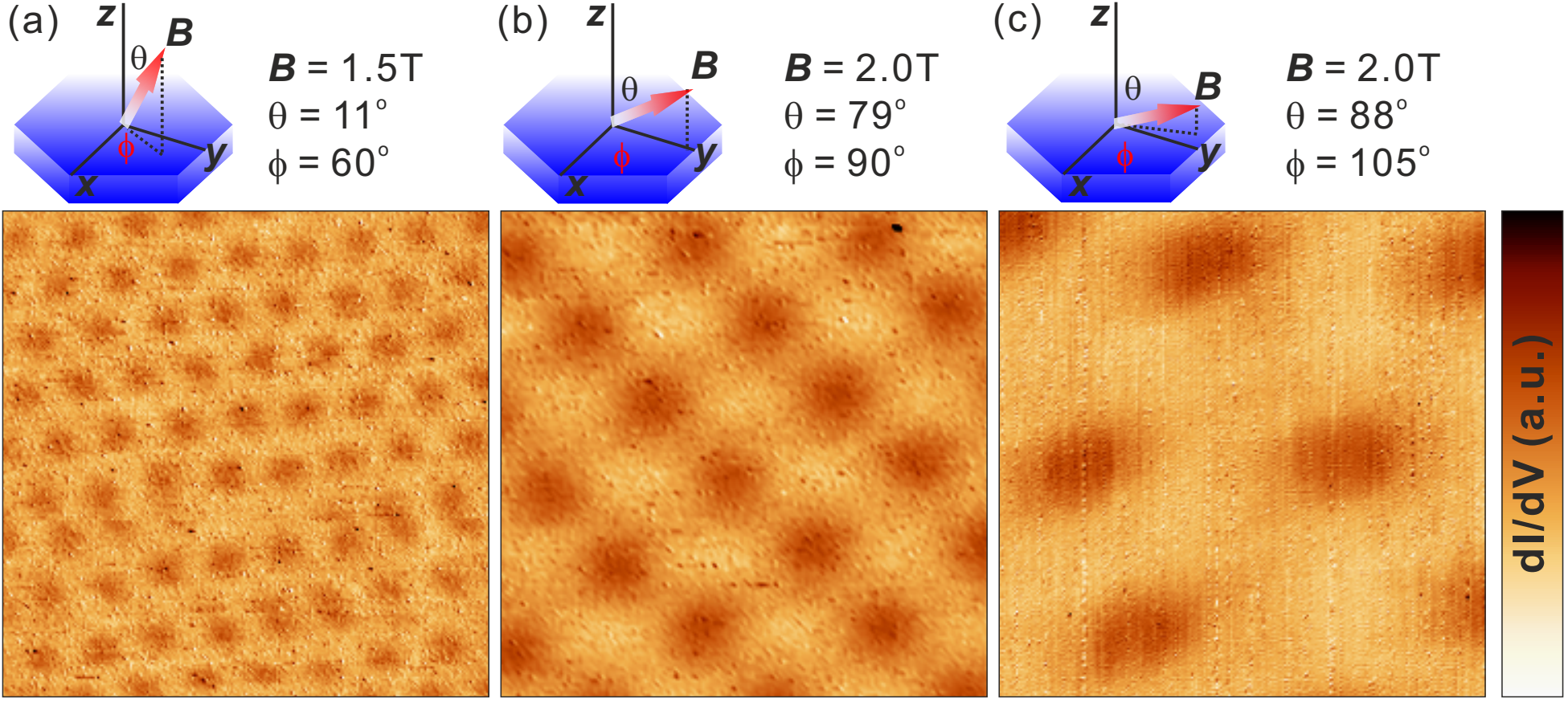
(a)
z
B
θ
ϕ
y
x
B = 1.5T
θ = 11°
ϕ = 60°
(b)
z
B
θ
ϕ
y
x
B = 2.0T
θ = 79°
ϕ = 90°
(c)
z
B
θ
ϕ
y
x
B = 2.0T
θ = 88°
ϕ = 105°
dI/dV (a.u.)